Attractive and Repulsive Intermolecular Interactions of a Polar Molecule: Short-Range Structure of Neat Supercritical CHF_3 Investigated by Raman Spectroscopy

Ken-ichi Saitow*

Department of Physics, Faculty of Science, Chiba University, Yayoi, Inage, Chiba 263-8522, Japan

Hideyuki Nakayama and Kikujiro Ishii

Department of Chemistry, Faculty of Science, Gakushuin University, Mejiro, Toshima, Tokyo 171-8588, Japan

Keiko Nishikawa

Division of Diversity Science, Graduate School of Science and Technology, Chiba University, Yayoi, Inage, Chiba 263-8522, Japan

Received: February 20, 2004; In Final Form: April 30, 2004

The short-range structure of the neat fluid of fluoroform (CHF_3) is investigated around the gas−liquid critical point by measurements of spontaneous Raman spectra of the C−F symmetric stretching (ν_2) and the C−F_3 symmetric deforming (ν_3) modes. The spectra are obtained at reduced temperatures $0.96 \leq T_r = T/T_c \leq 1.06$, the conditions of which permit isothermal studies in the gas, liquid, and supercritical states as functions of pressure and/or density. As the density increases, the spectral peaks shift toward the lower energy side and spectral widths become broader. In the supercritical region, the amount of shifting shows nonlinear density dependence, while the width becomes anomalously large. We analyze these density dependences along vibrational coordinates by the perturbed hard-sphere model. The amount of shifting is decomposed into attractive and repulsive components, and the changes of attractive and repulsive energies are evaluated as functions of density and packing fraction, both of which are continuously varied by a factor of 50. For both vibrational modes, the spectral shift consists principally of the attractive component at all densities and temperatures. Here we evaluate local density enhancement as a function of bulk density by the use of the values of attractive shift and by the use of dielectric analysis. Local density enhancement is highest at the bulk density, where the spectral width becomes anomolously broad. We analyze the density dependences of widths by comparing the experimental values with calculated homogeneous and inhomogeneous widths. The experimental results agree with the theoretical calculations. It is elucidated that the main contribution to width is density inhomogeneity. By comparing short-range structure studied in the present study with long-range structure previously studied by small-angle X-ray scattering, we found that the vibrational motion becomes significantly affected by the dielectric structure as the correlation length of the density fluctuation grows longer than the size of a first solvent shell of CHF_3. Under that situation, the ν_2 mode is more sensitive than the ν_3 mode to the dielectric structure in the vicinity of a vibrating molecule.

I. Introduction

The increasing use of supercritical fluids in a wide range of practical applications has motivated a number of recent attempts to understand the fundamental aspects of fluid structure. In the past few decades, supercritical fluid structures have been considered very inhomogeneous,[1−5] and this inhomogeneity is recently shown to be related to the efficiencies of extraction and chemical reaction. For example, solubility, rate constant, and yield of photochemical reaction, and relaxation times of electronic, vibrational, and rotational transitions each show an inflection, a minimum, or a maximum around the density where the inhomogeneity is greatest. The inhomogeneity of supercritical fluids has been expressed by different names, e.g., the aggregation, clustering, local density enhancement, and density fluctuation. The differences among these expressions depend on the system of fluids or the experimental and theoretical methodologies. In the present study, we distinguish the inhomogeneity according to spatial size, and define here that very long range, long range, and short range correspond to longer than a few micrometers, longer than a few nanometers, and the nearest neighbors of a molecule, respectively.

At close to the gas−liquid critical temperature, e.g., a reduced temperature $T_r = T/T_c \approx 1.00001$, very long-range inhomogeneity was observed. Several kinds of fluids were extensively investigated by static Rayleigh light scattering,[6−9] and the correlation length of density fluctuation of a few micrometers and transport coefficients were evaluated. At a temperature relatively far from the critical temperature ($T_r \geq 1.02$), long-range inhomogeneity has been recently studied by small-angle X-ray scattering (SAXS) and was characterized by both the correlation length of a few nanometers and the value of the density fluctuation.[10−12] To reveal dynamics of density inhomogeneity, the time evolution of inhomogeneously dispersed molecules has been investigated by dynamic light scattering.[13,14]

* Address correspondence to this author. E-mail: saitow@faculty.chiba-u.jp.

10.1021/jp049225c CCC: $27.50 © 2004 American Chemical Society
Published on Web 06/16/2004

The map of time constants of "critical slowing down" was recently produced as a contour curve on phase diagrams.[14]

As for the short-range inhomogeneity, static and dynamic structures in *supercritical solutions* have been extensively studied,[1,2] including the electronic absorption or emission spectrum,[15−17] time-resolved spectroscopy,[18−21] magnetic resonance,[22,23] and computer simulation.[24−26] The structure of a fluid around a solute molecule was well elucidated in several systems of supercritical solutions. On the other hand, there have been relatively few reports on the *short-range inhomogeneity of neat supercritical fluids* so far. One reason for the dearth of study on the short-range inhomogeneity of the neat fluids is experimental limitations, e.g., very high T_c and P_c of almost fluids, the electronic transition energy of fluid molecules located in a vacuum ultraviolet region, the small vibrational frequency shift as a function of density, and the relatively less structure of a radial distribution function near a critical point than normal liquid.

As a fundamental concept to express the short-range inhomogeneity of supercritical fluids, numerous researchers have used local density enhancement and/or local density augmentation.[1,2,15−17,24−39] For *neat fluids*, however, whether intermolecular interactions enhance local density has been discussed from theoretical and experimental approaches.[31−39] In theoretical studies, a Lennard-Jones (LJ) fluid investigation by molecular dynamics (MD) simulation first revealed local density enhancement as a function of bulk density.[31] A Monte Carlo (MC) simulation indicated either the subtle presence or the absence of local density enhancement in a LJ fluid.[32] Later, calculation by integral equations showed that the magnitude of local density enhancement depends significantly on the strength of intermolecular potentials,[33] and the difference of enhanced amounts of local densities between polar and nonpolar fluids has been theoretically elucidated by computer simulations.[34] As for experimental studies, the analysis of the Raman spectral shift of a polar molecule showed the existence of local density enhancement,[35] which was also observed by terahertz absorption spectroscopy.[36] The linear density dependence of the Raman shift of supercritical ethane was recognized as a lack of local density enhancement.[38,39] Accordingly, local density enhancement shows different features in neat supercritical fluids, depending on the systems or methodologies used. Long-range inhomogeneity, however, exists in almost all neat systems,[3−14] and this universality has been understood to be responsible for the principle of corresponding state.[3]

Our research interests are the following. First is how the short-range inhomogeneity depends on the systems being used. Second is how the short-range structure is related to the long-range one. Third is how different vibrational modes are affected by the same dielectric surrounding. To obtain clues to these questions, we measured the vibrational Raman spectrum of fluoroform (CHF_3), because of the advantages that its molecule offers. First, the small and simple CHF_3 molecule has been well studied by molecular spectroscopy and theoretical calculation. The information from these studies enables us to analyze spectra in detail. Second, the CHF_3 molecule is a typical polar molecule and has a large dipole moment (1.65 D).[40] The data for a polar molecule are compared with systems of nonpolar molecules. Third, our previous studies investigated the long-range inhomogeneity of supercritical CHF_3.[10,14] These results are available for comparison with the results of short-range inhomogeneity obtained from the present study under the same conditions of thermodynamic states—namely temperature, pressure, and density. Fourth, since supercritical CHF_3 has been frequently used as a typical solvent for studies of supercritical solutions,[1,2] the results given by many researchers offer much useful information to the present study.

In the present study, we measured the symmetric C−F stretching (ν_2) and the symmetric C−F_3 deforming (ν_3) modes of CHF_3 at isothermal conditions $0.96 \leq T_r = T/T_c \leq 1.06$. In the range of temperature, the local structure near a vibrating molecule in the supercritical state was compared with that in the gas or liquid states below the critical temperature. Neither of the two measured vibrational modes has the Fermi resonance components.[41,42] As a result, the analysis of these modes becomes relatively easier than that of symmetric C−H stretching (ν_1) of CHF_3 with the Fermi resonance components.[42] The peak shift and spectral broadening obtained from Raman spectra were analyzed by using the perturbed hard-sphere model. Intermolecular interactions affecting the shifting and the broadening were studied by decomposing the interactions into attractive and repulsive interactions. Thus, the short-range structure around a vibrating molecule was elucidated by the evaluations of the attractive and repulsive energies as a function of density, varied by a factor of 50. The short-range structure observed by vibrational spectroscopy was discussed in comparison with long-range structure observed by the X-ray scattering at the same densities and temperatures.

II. Experimental Section

The light source for Raman measurements was an argon-ion laser operated at a single line of 514.5 nm at a power of 200 mW in front of an optical cell. The scattering light was collected by lenses and introduced into a monochromator (TRIAX 550, JovinYbon-Spex) equipped with a charge-coupled device (CCD) camera after passing through a supernotch filter (Kaiser Optics) to remove Rayleigh scattering. The optical configuration among the light source, sample cell, and detection system was set to ss-polarization with use of a half-wave plate and polarizers.

The sample cell was one specially constructed for high-pressure conditions.[35,43] It was made of stainless steel SUS304 with 7-mm-thick glass windows. The cell was designed to withstand 400 K and 30 MPa. The sample fluid was sealed by a Kalrez O-ring, and the pressure was adjusted to 25 MPa with an injector (AKICO). The pressure was monitored with a strain gauge backed up with a strain amplifier (Kyowa Dengyo). The temperature of the sample was controlled by circulating water from a chillier unit to a water jacket, and was monitored by a thermocouple. Fluctuations of pressure and temperature were suppressed to within ±0.1% during measurement.

The chemical purity of CHF_3 was commercially guaranteed to be 99.99%. The fluid was filtrated with a PTFE membrane filter with a pore size of 0.1 μm (Advantec) in a high-pressure container (Millipore) to raise optical purity. The critical constants of CHF_3 are reported to be $T_c = 299.06$ K, $P_c = 4.836$ MPa, and $\rho_c = 0.525$ g cm^{-3}.[44] The studied thermodynamic states are plotted on the $P-T$ phase diagram in Figure 1a along six isotherms of reduced temperatures $0.96 \leq T_r \leq 1.06$. The corresponding densities are also shown in Figure 1b; these densities are calculated from the empirical state equation[44] by the use of measured P and T values.

Under the conditions mentioned above, Raman spectra of ν_2 and ν_3 modes were measured at densities that varied by a factor of 50. In the present study, an instrumental function of the Raman spectrometer was obtained by measuring the emission line of an Ne lamp. The spectral shape of the instrumental function was characterized by Lorentzian function with the full width at half-maximum (fwhm) of 1 cm^{-1}. The wavenumber

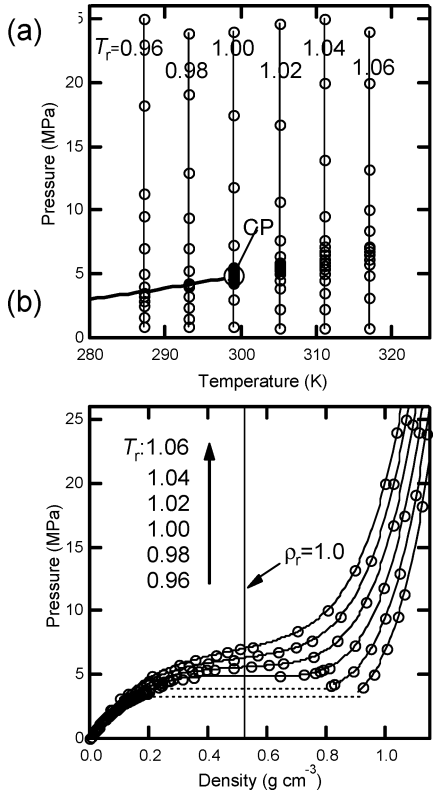

Figure 1. Measured thermodynamic states of Raman spectra of fluoroform (CHF_3) plotted on a (a) $P-T$ phase diagram and a (b) $\rho-P$ phase diagram. The critical point is represented as CP. Values as in 0.96−1.06 indicate reduced temperatures described as $T_r = T/T_c$. Measurements are carried out along these isotherm lines by increasing pressures.

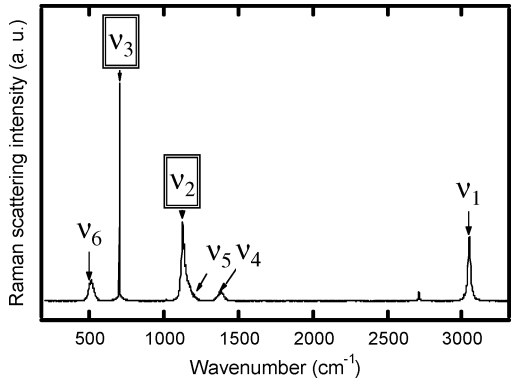

Figure 2. Typical example of a Raman spectrum of the fundamental vibrational modes of CHF_3 in a measured supercritical state. Raman bands of ν_1, ν_2, ν_3, ν_4, ν_5, and ν_6 are assigned to C−H symmetric stretching, C−F symmetric stretching, $C-F_3$ symmetric deforming, C−H bend, C−F antisymmetric stretching, and $C-F_3$ antisymmetric deforming modes, respectively (ref 45).

values on all measured Raman spectra were calibrated by the emission lines of the Ne lamp.

III. Results

III.A. Typical Spectra of CHF_3 at the Gas, Liquid, and Supercritical States. Figure 2 shows a typical Raman spectrum of the supercritical CHF_3 from 300 to 3300 cm^{-1} ($T_r = 1.02$ and $P = 5.84$ MPa). In the present study, the measurements and analyses are concentrated in the ν_2 and ν_3 modes. Figure 3 shows polarization dependences of Raman spectra of both vibrational modes. Since the insignificant depolarization components are observed by a p−s polarized configuration, both

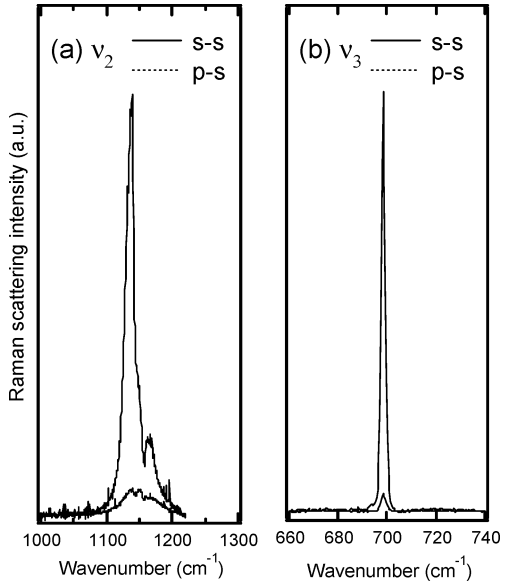

Figure 3. Polarization dependences of vibrational Raman spectra of ν_2 and ν_3 modes. The notations of s−s and p−s represent the configuration of s−s polarization between incident and scattering light and the p−s configuration, respectively.

of these spectra consist of a Q-branch and negligible P and R ones. As a result, we are able to treat the spectra of ν_2 and ν_3 modes as isotropic bands, which are measured on the same polarization between the incident and scattering lights, that is, s−s polarization.

For typical results below and above T_c, the spectra of ν_2 and ν_3 modes at $T_r = 0.96$ and those at 1.02 are shown in Figures 4a, b and 5a,b, respectively. As common features in ν_2 and ν_3 bands, the peak positions of spectra shift toward the lower energy side, and the spectral width broadens with the increase of pressure or density.

III.B. Spectral Width and Peak Position as Functions of Pressure or Density. The spectral width and peak position are investigated as functions of pressure and density. The measured spectra of ν_2 and ν_3 modes are analyzed by the Gaussian function convoluted with the instrumental function in the calibrated wavelength region. Thus, the deconvoluted spectral widths and peak positions on the corrected wavenumber are obtained to allow us to discuss carefully those pressure or density dependences. The spectra of the ν_2 mode show slightly antisymmetric shapes, because the right wing partially overlaps with the weak band of the antisymmetric C−F stretching mode (ν_5) around 1160 cm^{-1}. The spectrum around 1100 cm^{-1} is decomposed into bands of ν_2 and ν_5 modes, and the width and peak position of the ν_2 mode are acquired.

Panels a and b in Figure 6 summarize fwhm of the ν_2 and ν_3 modes, respectively, as a function of pressure in the temperature range of $0.96 \leq T_r \leq 1.06$. For the data of isotherms at $T_r = 0.96$ and 0.98, the width gradually increases in the gas state with the increase of pressure. At the positions where the isothermal curves cross the vapor−liquid coexistence curve, the widths show discontinuities. This obviously arises from a first-order phase transition from the gas to liquid states. The width in the liquid state becomes constant within the present pressure range. In the supercritical region the width also becomes constant, and a plateau appears in high-pressure sides. Note that the profiles of spectral widths in the low- and high-pressure regions in the supercritical state are analogous to those in the gas and liquid states, respectively. These experimental results show that local structures around a vibrating molecule in the

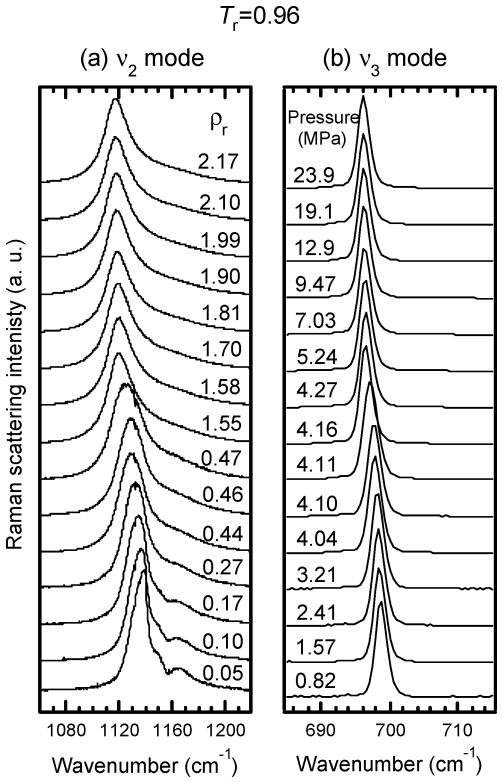

Figure 4. (a) Vibrational Raman spectra of the ν_2 mode of CHF_3 at gas and liquid states at the reduced temperature $T_r = 0.98$. (b) Spectra of the ν_3 mode at the same thermodynamic conditions as those of panel a. The spectra of ν_2 and ν_3 modes are measured at the same pressures, and the corresponding reduced densities $\rho_r = \rho/\rho_c$ are also given at the left.

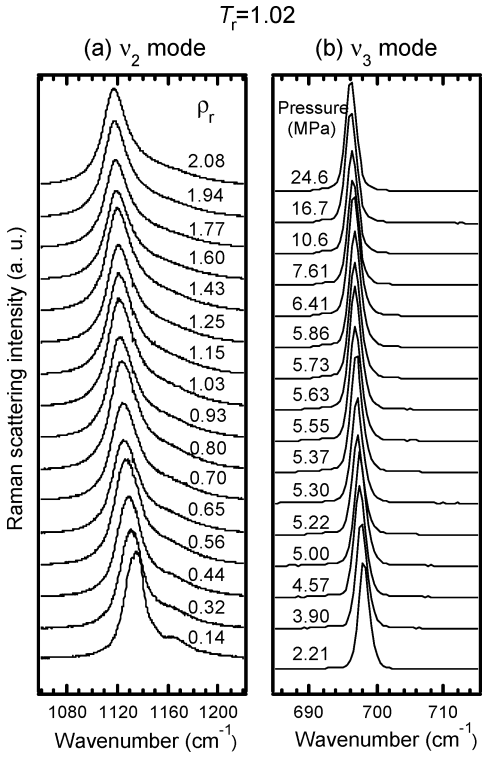

Figure 5. (a) Vibrational Raman spectra of the ν_2 mode of CHF_3 at supercritical states of $T_r = 1.02$. (b) Spectra of the ν_3 mode at the same thermodynamic conditions as those of panel a. The spectra of ν_2 and ν_3 modes are measured at the same pressures, and the corresponding reduced densities ρ_r are also given.

lower and higher pressure regions of the supercritical state are similar to those of gas and liquid states, respectively. This tends to agree with our previous results on the vibrational Raman of neat supercritical CO_2.[43]

To examine the density dependence of a spectrum, the width and peak position for the spectra of ν_2 and ν_3 modes are shown in Figure 7, panels a and b, respectively, at several temperatures as functions of the reduced density $\rho_r = \rho/\rho_c$. It is seen that the spectral widths of the ν_2 mode become much larger than those of the ν_3 mode. Blank regions correspond to the discontinuity of density due to the phase transition. In all data obtained above the critical temperature, the width sublinearly increases in the low-density region, and an anomaly successively appears around $\rho_r = 0.7$. The width gradually tends to become constant in the high-density region, and the plateau appears in higher density regardless of the increase in density.

As for the position of the peak, the spectra of ν_2 and ν_3 modes shift toward the lower energy side as the density increases. The amount of the shift is much larger in the ν_2 mode than in the ν_3 mode. In particular, it should be noted that the shift amount of the ν_2 mode is about 20 cm^{-1} at around $\rho_r = 2$. This value is significantly large, because studies of most reported molecules show shift amounts at around $\rho_r = 2$ to be about a few to 10 cm^{-1} at most in neat fluids as well as supercritical solutions. Another feature of the peak positions is that the shift amounts of both modes are inflected around $\rho_r = 0.8$. The density at the inflections is nearly equal to the density giving anomaly of spectral widths. According to experimental results for these density dependences, a local structure in the vicinity of a vibrating molecule significantly changes around the bulk density of $\rho_r = 0.7-0.8$.

III.C. Correlation between Spectral Shift and Macroscopic Dielectric Structure. To investigate the short-range structure from a dielectric point of view, we examined the spectral shift by using Onsager's reaction field theory. According to the theory, a medium with a large dielectric constant stabilizes an excited state more than the ground state by the larger dipole moment of the excited state, and this stabilization causes a red shift in the spectrum.[46,47] According to this idea, the red-shifted vibrational spectra of acetone in supercritical CO_2 were examined as a function of the reaction field.[48] In a case of supercritical CHF_3 as a polar molecule, spectral shift was analyzed by the following reaction field,[15]

$$\frac{\Delta\nu}{\nu_0} = c\left(\frac{\epsilon - 1}{\epsilon + 2} - \frac{n^2 - 1}{n^2 + 2}\right) \quad (1)$$

where the $\Delta\nu/\nu_0$ is a solvent-induced frequency shift normalized by the gas-phase frequency, C is the constant depending on properties of a molecule, $(\epsilon - 1)/(\epsilon + 2) - (n^2 - 1)/(n^2 + 2)$ is the reaction field, ϵ is the dielectric constant, and n is the refractive index. In the present study, the vibrational spectral shift is analyzed by the use of this reaction field.

Figure 8 shows the shifts at $T_r = 1.02$ as functions of the reaction field. The plotted data indicate the percentage of the amount shifted from the position of the Raman spectrum at the isolated condition. Dielectric constants and refractive indices for the reaction fields at each density are used as values obtained from our measurements (vide infra).[49,50] As shown in Figure 8, nonlinear features appear as a value of the reaction field less than 0.5. The nonlinearity indicates a deviation of dielectric structure around a vibrating molecule from an averaged dielectric one. A similar nonlinearity of less than 0.5 at the reaction field was observed in the shift in the electronic transition

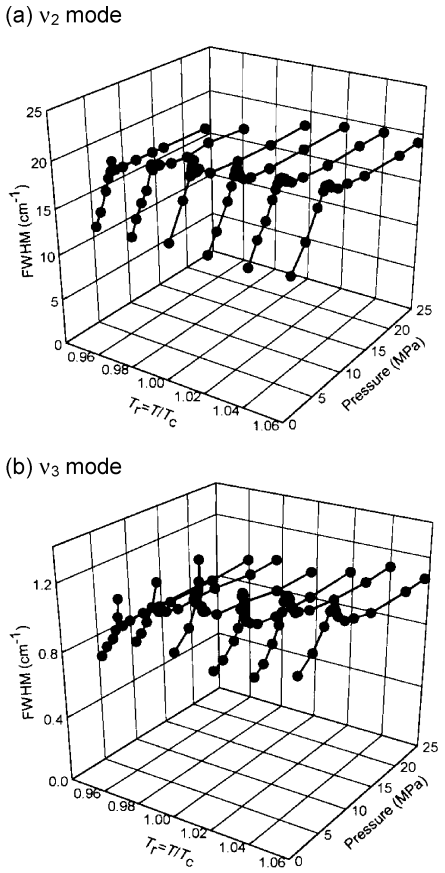

Figure 6. Spectral widths of (a) the ν_2 mode and (b) the ν_3 mode in gas, liquid, and supercritical states as functions of pressure and reduced temperatures $0.96 \leq T_r \leq 1.06$.

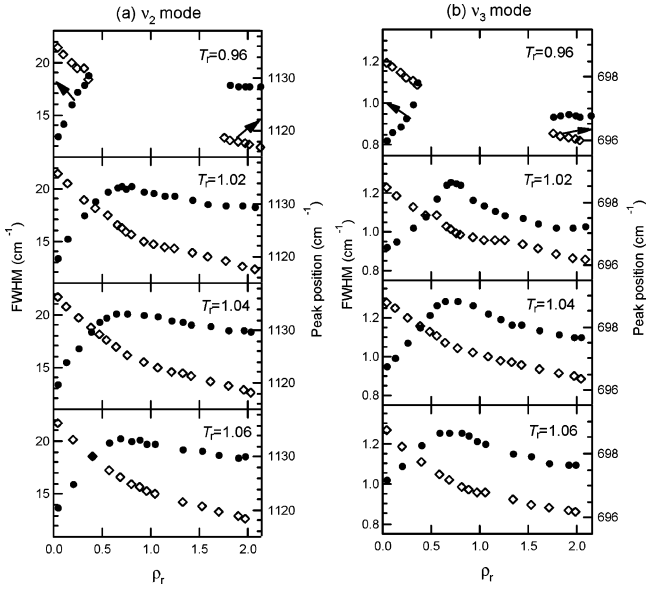

Figure 7. (a) Density dependence of spectral width (●) and peak positions (◊) of ν_2 measured along the isotherm conditions at the reduced temperatures $T_r = 0.96$, 1.02, 1.04, and 1.06. (b) Density dependence of spectral width (●) and peak positions (◊) of ν_3 at the same thermodynamic conditions against panel a.

of CHF_3's supercritical solution. This deviation from the linear trend was interpreted as a local density enhancement around a solute molecule.[15] Another feature of Figure 8 is that the amount of shift is much larger in the ν_2 mode than in the ν_3 mode. In addition, a deviation from the linear line becomes notable in the ν_2 mode. These results mean that the stretching mode, in

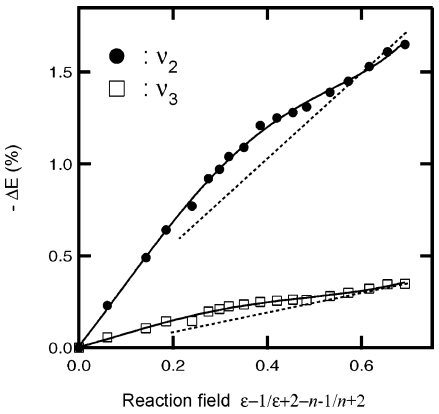

Figure 8. Spectral shift (%) from the isolated condition at the reduced temperature $T_r = 1.02$ as a function of the Onsager reaction field. The solid circles and squares are the peak position of ν_2 and ν_3 modes, respectively. The solid curve and the dashed line are a fitting curve of the polynominal function and act as a guide for eye and the linear line is due to the nature of the average dielectric structure, respectively.

contrast to the deforming one, is specifically affected by the dielectric structure around a vibrating molecule at the same density and temperature.

IV. Theoretical Background for Analysis of Raman Spectra as a Function of Density

IV.A. Spectral Shift Decomposed into Attractive and Repulsive Shifts. As isolated molecules condense, an average force exerted by surrounding molecules shifts the vibrational frequency. On the basis of a theoretical model developed by Schweizer and Chandler (SC model),[51] the density dependence of a vibrational Raman spectrum has been excellently analyzed in high-pressure conditions: neat liquids or solutions in GPa[51−57] and supercritical fluids in MPa.[35,58,59] In this model, the frequency shift $\Delta\nu$ can be partitioned into contributions from the repulsive and attractive components, as follows,

$$\Delta\nu = \Delta\nu_R + \Delta\nu_A \tag{2}$$

where the $\Delta\nu$, $\Delta\nu_R$, and $\Delta\nu_A$ are the net, repulsive, and attractive frequency shifts, respectively. The repulsive and attractive shifts become positive and negative values, respectively. The repulsive contribution is calculated by using a hard-sphere approximation, and the attractive contribution is empirically derived by subtracting the repulsive shift from the experimentally obtained net shift. In this model, a solvent molecule and a solute molecule have been characterized by a hard sphere and a pseudodiatomic molecule composed of two hard-sphere atoms, respectively.[51−57] For neat fluids, the solute and solvent molecules are the same, but are treated as a vibrating molecule and a hard sphere, respectively.[35,51,53,55,58,59]

In the SC model, the repulsive spectral shift, $\Delta\nu_R$, is expressed as follows,

$$\Delta\nu_R \approx \nu_0 \frac{F_R}{f}\left[-\left(\frac{3g}{f}\right)+\left(\frac{G_R}{F_R}\right)\right] \tag{3}$$

where ν_0 is the vibrational frequency of the isolated molecule, f and g are the intramolecular quadratic harmonic and cubic anharmonic force constants of the solute molecule,[60] and F_R and G_R are the linear and quadratic constants respectively indicating forces exerted by solvent molecules along the normal coordinate of solute.[61,62] A similar theoretical model was later developed by Zakin and Herschbach. That model, called the

TABLE 1: Parameters for Calculation of Spectral Shift and Width

parameters	ν_2	ν_3
f (a J Å^{-2})[a]	8.4	3.4
g (a J Å^{-3})[a]	30.9	2.5
G_R/F_R[b]	1.0	1.2
m_1[c]	2.77	2.74
m_2[c]	4.40	4.41
m_3[c]	4.43	4.35
b_1[c]	−1.21	−1.04
b_2[c]	−2.74	−2.42
b_3[c]	−3.61	−3.30
σ_s (Å)[d]	4.3	4.3
σ (Å)[d]	3.0	3.3
σ_1 (Å)[d]	3.9	3.8
σ_2 (Å)[d]	2.2	2.8
L (Å)[b]	0.23	0.23
ω_e (cm^{-1})[a]	1154.7	709.7

[a] Reference 60. [b] References 61 and 62. [c] Reference 52. [d] Reference 63.

perturbed hard-sphere model, has been conveniently rewritten to obtain the density dependence, and it is used for the present calculations,[52,53]

$$\frac{\Delta\nu_R}{\nu_0} = c_1 \exp(m_1\rho^*) + c_2 \exp(m_2\rho^*) - c_3 \exp(m_3\rho^*) \quad (4)$$

with

$$c_k = k\alpha_R\theta z(1-z)^{k-1} \exp b_k \quad (5)$$

and

$$\alpha_R = r_e\left[-\frac{3}{2}\left(\frac{g}{f}\right) + \left(\frac{G_R}{F_R}\right)\right] \quad (6)$$

where the coefficients m_k and b_k are empirical parameters,[52] depending on the molecular size, and the density is ρ^* represented as follows

$$\rho^* = \rho\sigma_s^3 \quad (7)$$

where ρ is the number density and σ_s is the diameter of the solvent hard sphere. The value of θ is given by

$$\theta = \frac{k_B T}{f r_e^2} \quad (8)$$

where the k_B is the Bolzmann constant and r_e the equilibrium bond length. The value of z is expressed as

$$z = \frac{r_e}{\sigma} \quad (9)$$

where the σ is the van der Waals size of the solute molecule. Thus, we calculate the repulsive shift using eq 4 as a function of density. The calculation parameters are listed in Table 1. The attractive shift is derived by subtracting the calculated repulsive shift from the net shift of the experimental data.

IV.B. Homogeneous and Inhomogeneous Broadening of Vibrational Bands. A vibrational spectral width involves the fluctuation of vibrational frequency due to the fluctuation of molecular interactions. The frequency fluctuation can be characterized by a root-mean-square amplitude and by a correlation time describing vibrational motions.[64,65] In the slow-motion limit the broadening is inhomogeneous, and the line width and shape show a static probability distribution of frequency fluctuations; this distribution becomes Gaussian. In the fast modulation limit, on the other hand, the broadening is homogeneous and the spectral shape is expressed by the Lorentzian. The actual vibrational spectrum is the convolution of a homogeneously broadened shape from rapidly varying repulsive force fluctuations and an inhomogeneously broadened one from slowly varying attractive force fluctuation. The SC model partitions solvent force fluctuations into the attractive and repulsive contributions as a function of density. In this model, the inhomogeneous and homogeneous widths are expressed by the use of the former and latter contributions, respectively.[51] We analyze width by calculating homogeneous and inhomogeneous widths in the following manner.

In a homogeneous case in the SC model, a hard-sphere/Enskog collision is used as the model of repulsive interactions.[51] In this case, a pure dephasing rate characterizing spectral width is described in the condition of homogeneous limit as follows

$$\tau_R^{-1} = 2\left(\frac{\Delta q}{\hbar}\right)^2 3k_B T\frac{1}{2}\left(1 + \frac{r_e}{2}\left(\frac{1}{\bar{\sigma}_1} + \frac{1}{\bar{\sigma}_2}\right)\right)(m_1\lambda_1^2\tau_{E1}^{-1} + m_2\lambda_2^2\tau_{E2}^{-1}) \quad (10)$$

with

$$\Delta q = (Q_{11} - Q_{00}) + \frac{(Q_{11}^2 - Q_{00}^2)}{4L} = \frac{g\hbar}{2\mu^2\omega_e^3} + \frac{\hbar/2\mu\omega_e}{4L} \quad (11)$$

where the $\bar{\sigma}_i$ is the average size of an atom i of a pseudodiatomic solute molecule, as in $\bar{\sigma}_i = (\sigma_i + \sigma_s)/2$, m_i is the mass of the atom i in the solute molecule, λ_i is the steric factor as in $[1 - (r_e/2\sigma_i)^2]/2[1 + (r_e/2\sigma_i)]$, Q_{jj} is the vibrational amplitude,[51,64,65] L is the characteristic range parameter for repulsive interaction,[61,62] μ is the reduced mass of solute, and ω_e is the harmonic frequency. The Enskog collision rate τ_{Ei}^{-1} between hard spheres is expressed as follows

$$\tau_{Ei}^{-1} = \frac{8}{3}\sqrt{\frac{\pi k_B T}{2\mu_i}}\rho\sigma_i^2 g(\sigma_i) \quad (12)$$

where the μ_i is the reduced mass between atom i of solute and the solvent, as in $\mu_i^{-1} = m_i^{-1} + M^{-1}$, and $g(\sigma_i)$ is the contact value of the radial distribution function for solute and solvent molecules as follows[51]

$$g(\sigma_i) = \frac{1}{2}(1-\eta)^{-3}\sum_i \{(1-\eta)[(\sigma_i/\bar{\sigma}_i)(1+2\eta) + (\sigma_s/\bar{\sigma}_i)(1-\eta) + \eta^2(\sigma_i/\bar{\sigma}_i)^2\} \quad (13)$$

where η is the packing fraction as $\pi\rho\sigma_s^3/6$. Thus, the line width δ_R due to the pure dephasing is expressed at the homogeneous limit as follows

$$\delta_R = 2\tau_R^{-1}/2\pi c \quad (14)$$

where c is the speed of light.

The slowly varying force giving the inhomogeneous width is expressed in the SC model as follows[51]

$$\tau_A^{-1} \approx |\Delta\nu_A|\sqrt{\frac{\langle\Delta N\rangle^2}{N^2}} \quad (15)$$

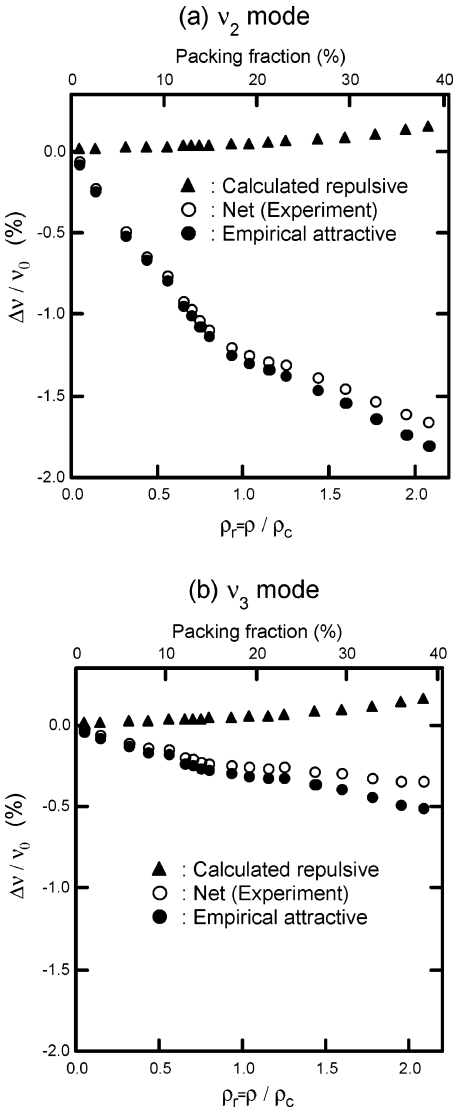

Figure 9. Spectral shifts of ν_2 and ν_3 modes at the reduced temperature $T_r = 1.02$ as a function of packing fraction and reduced density ρ_r. The solid triangles, open circles, and solid circles are repulsive, net, and attractive spectral shifts, respectively.

where $\Delta\nu_A$ is the amount of attractive shift, N is the average number of molecules in a local volume, and ΔN is the difference between the average and the effective numbers of molecules in the volume. The inhomogeneous width δ_A with Gaussian distribution is expressed as follows

$$\delta_A = 2\sqrt{\ln 2}\ \tau_A^{-1}/2\pi c \tag{16}$$

V. Discussion

V.A. Attractive and Repulsive Components in Spectral Shifts. Figure 9 shows the measured net shift, the calculated repulsive shift, and the empirical attractive shift as functions of reduced density and/or packing fraction at the isothermal condition of $T_r = 1.02$. The attractive components decrease as molecules are condensed, whereas the repulsive ones increase. The shift amounts are listed in Table 2, which shows that the repulsive shift becomes similar in both vibrational modes. Let us examine the calculated repulsive shift in comparison with those of other reported fluids.[51,53,55,57,58] Table 3 summarizes the repulsive shifts for several vibrational modes in high-pressure conditions. To compare clearly the other fluids with the present one, the reported data are rewritten by normalizing each shift from the isolated condition (%) as a function of reduced density ρ_r. By extrapolating those values, it is confirmed that the amounts of the repulsive shifts in almost all systems reach about 0.05% at $\rho_r = 1$ and 0.2% at $\rho_r = 2$, and the present values are also in accordance with those values. Such accordance is attributable to the use of the hard-sphere model in all the studies. Also, the calculated values in the present study are appropriate for application to the hard-sphere model.

As for the attractive component, Figure 9 shows that the value of an attractive shift becomes larger than that of a repulsive one in both modes. This means that the measured Raman spectra consist principally of the attractive component in the present density ranges. Another feature of Figure 9 is that the amount of attractive shift shows nonlinear density dependence and is inflected around $\rho_r = 0.8$. According to the SC model, the attractive shift is linearly proportional to the density in a homogeneous (uniform) distribution of molecules, as follows

$$\Delta\nu_A = C_a\rho \tag{17}$$

where C_a is an attractive shift parameter. When this condition is applied to the present system, it can be considered that a deviation from the linear trend is due to density inhomogeneity, because aggregations of molecules are able to cause a greater attractive shift than the uniform molecular distribution.

V.B. Local Density Enhancement Induced by Attractive Intermolecular Interactions. In supercritical solutions, a deviation from a linear trend as a function of density has been observed in a number of studies on spectral shift, partial molar volume, local coordination number of a molecule, and so on.[1,2,15−17,24−31] Such deviations from the linear lines are attributed to an enhancement of local density around a solute molecule. The enhancement is expressed as follows

$$\langle\delta\rho_l\rangle = \langle\rho_l - \langle\rho\rangle\rangle \tag{18}$$

where $\delta\rho_l$, ρ_l, and $\langle\rho\rangle$ are the local density enhancement, local (effective) density, and the bulk (averaged) density, respectively. In these studies, the value of enhancement has been evaluated by the following procedures. A local density is generally estimated by finding the density that gives the same amount of shift on a linear line as it does on a nonlinear curve, as shown in Figure 10. The enhancement is given by the difference between the density on the curve and that on the linear line. The obtained values correspond to an ensemble average whose value reflects the density inhomogeneity locally enhanced by molecular aggregations. We then estimate the local density enhancement according to these procedures. Note that the local density enhancement in the present study enables us to acquire the value arising from attractive intermolecular interactions only. That is, we are able to investigate the *attractive* interactions under the condition of the absence of *repulsive* intermolecular interaction by the use of the attractive spectral shift. The obtained local density enhancement thus directly reflects a portion of the molecules attractively aggregated.

Figure 11c shows the local density enhancement of supercritical CHF_3, which is obtained from the deviation from the linear line. The enhancement is observed in the neat fluid, and the maximum value appears at around $\rho_r = 0.8$. Let us discuss the following effect: a large enhancement might change the values of repulsive shift by increasing the local density and might result in changes in the values of attractive shift and local density enhancement. We recalculated the repulsive and attractive shifts using the local density, which was obtained from the summation of bulk density and the

TABLE 2: Shift Amounts of Experimental Net, Calculated Repulsive, and Empirical Attractive Shifts as a Function of Pressure, Density, and Packing Fraction at Reduced Temperature $T_r = T/T_c = 1.02$

				ν_2			ν_3		
pressure (MPa)	ρ (g cm^{-3})	$\rho_r = \rho/\rho_c$	packing fraction (%)	$\Delta\nu/\nu_0$ (%)	$\Delta\nu_R/\nu_0$ (%)	$\Delta\nu_A/\nu_0$ (%)	$\Delta\nu/\nu_0$ (%)	$\Delta\nu_R/\nu_0$ (%)	$\Delta\nu_A/\nu_0$ (%)
0.80	0.02	0.05	0.8	−0.06	0.018	−0.08	−0.020	0.020	−0.040
2.21	0.07	0.14	2.6	−0.23	0.019	−0.25	−0.056	0.022	−0.078
3.90	0.17	0.32	5.9	−0.49	0.023	−0.52	−0.106	0.026	−0.132
4.57	0.23	0.44	8.1	−0.64	0.026	−0.67	−0.143	0.029	−0.172
5.00	0.29	0.56	10.3	−0.77	0.030	−0.80	−0.145	0.033	−0.178
5.22	0.34	0.65	12.1	−0.92	0.033	−0.95	−0.196	0.037	−0.233
5.30	0.37	0.70	13.0	−0.97	0.035	−1.00	−0.210	0.038	−0.249
5.37	0.39	0.75	13.9	−1.04	0.036	−1.07	−0.226	0.040	−0.266
5.43	0.42	0.80	14.8	−1.09	0.038	−1.13	−0.235	0.042	−0.277
5.55	0.49	0.93	17.2	−1.21	0.044	−1.25	−0.249	0.049	−0.298
5.63	0.54	1.04	19.2	−1.25	0.049	−1.30	−0.256	0.054	−0.310
5.73	0.60	1.15	21.3	−1.28	0.055	−1.34	−0.261	0.061	−0.321
5.86	0.66	1.25	23.1	−1.31	0.062	−1.37	−0.259	0.068	−0.327
6.41	0.75	1.43	26.5	−1.39	0.075	−1.47	−0.281	0.082	−0.363
7.61	0.84	1.60	29.5	−1.45	0.089	−1.54	−0.299	0.097	−0.396
10.63	0.93	1.77	32.8	−1.53	0.108	−1.64	−0.321	0.118	−0.438
16.67	1.02	1.95	36.1	−1.61	0.131	−1.74	−0.345	0.142	−0.487
24.58	1.09	2.08	38.5	−1.65	0.151	−1.81	−0.348	0.163	−0.511

TABLE 3: Vibrational Frequency Shifts of Calculated Repulsive and Empirical Attractive Shifts of Various Fluids at High-Pressure Conditions Analyzed by the SC Model

molecule	mode	sample condition	density ($\rho_r = \rho/\rho_c$)	repulsive shift (%)	attractive shift (%)
cyclohexane[a]	C—H stretch	in supercritical CO_2	0.29	0.014	−0.04
			0.87	0.055	−0.11
			1.70	0.147	−0.22
isobutylene[b]	C═C stretch	liquid	2.51	0.124	−0.53
			2.79	0.162	−0.59
			2.93	0.185	−0.62
	C—C stretch		2.51	0.512	−0.39
			2.79	1.073	−0.50
acetone[b]	C═O stretch	liquid	2.87	0.111	−1.44
			3.48	0.193	−1.74
furan[c]	bending	liquid	3.07	0.43	−0.40
			3.14	0.48	−0.41
			3.25	0.52	−0.43
	C—H stretch		3.07	0.63	−0.82
			3.25	0.70	−0.90
methanol[d]	C—H stretch	liquid	3.08	0.245	−0.17
			3.24	0.262	−0.21
			3.35	0.300	−0.25
$CHCl_3$[e]	C—H stretch	in CS_2 liquid	2.87	0.60	−1.25
			3.20	0.70	−1.30
			3.54	0.80	−1.45
n-buthanol[e]	O—H stretch	in CS_2 liquid	2.87	0.55	−1.80
			3.20	0.65	−2.00
			3.54	0.75	−2.20

[a] Reference 58. [b] Reference 51. [c] Reference 55. [d] Reference 57. [e] Reference 53.

enhancement of local density. As a result, the increase in repulsive shift by the effect becomes small in the present density range, and the increased amounts for ν_2 and ν_3 modes are calculated to be less than 0.05% and 0.02%, respectively, even at the density where the enhancement becomes maximum. Therefore, it is safe to say that the changes in repulsive and attractive shifts by the effect are negligible in the present density range. In contrast, when molecules are compressed to a density around $\rho_r = 3$, the repulsive shift increases significantly, owing to the exponential part of eq 4.

To further discuss the value of local density enhancement, we also estimated local density enhancement by another analysis. In this analysis, the local density enhancement was obtained from the difference between two curves, which were the attractive shift and the reaction field as a function of density (vide supra), as shown in Figure 11. The obtained local density enhancement is shown in Figure 11c. It is obvious that the enhancement is also observed in this analysis. By comparing to two values of Figures 10c and 11c, the latter is smaller than the former. This difference is ascribed to each deviation amount: the deviation from the linear line in Figure 10 and the deviation from the curve in Figure 11. Let us discuss this briefly. The value of the local density enhancement in Figure 10 is evaluated from the attractive shift treated to be due to mainly dispersion, whose intermolecular interaction is considered to be linear against the density. On the other hand, the value in Figure 11 is obtained from the attractive shift incorporating dielectric interactions such as dipole−dipole interaction in polar molecules, which is considered to be nonlinear against the density. As shown in Figure 11, the reaction field is slightly nonlinear against the density. This subtle nonlinearity results in the decreased amount of enhancement in Figure 10. We compared two local density enhancements in this study with the local density enhancement investigated by simulation of

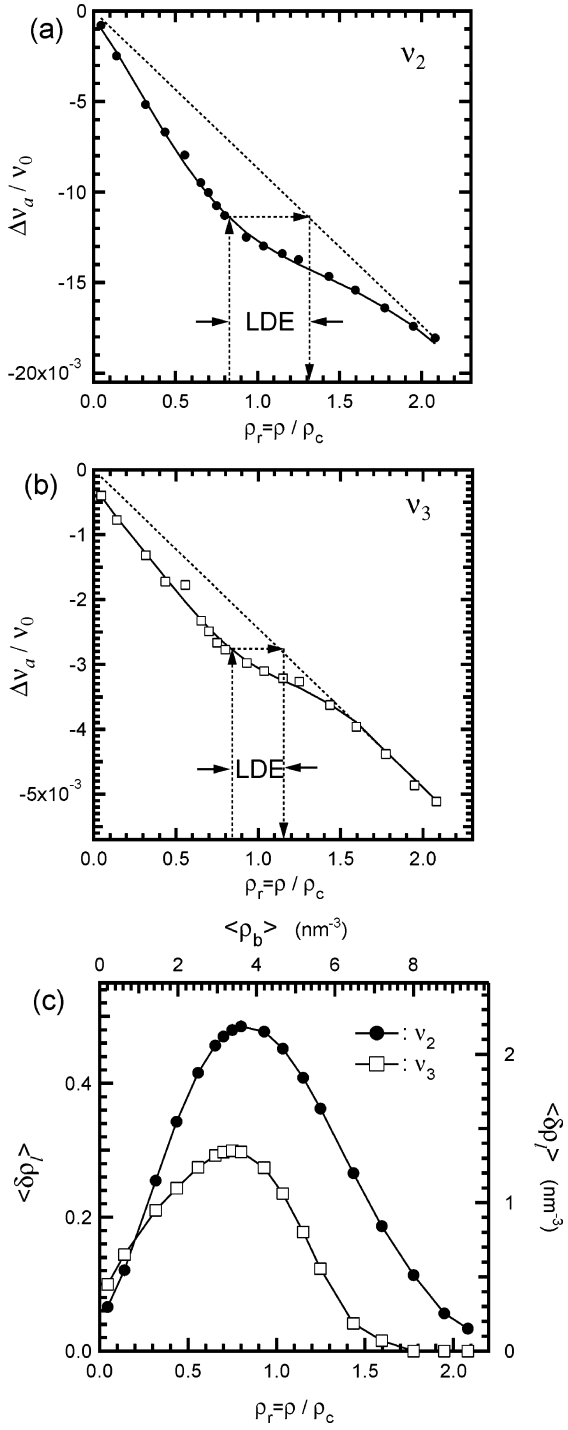

Figure 10. Attractive shift of (a) ν_2 and (b) ν_3 modes at the reduced temperature $T_r = 1.02$ as a function of reduced density ρ_r. The solid curve is a fitting curve of the polynominal function and acts as a guide for the eye. (c) Local density enhancement (LDE) in the neat condition. Units of the local density enhancement and bulk density are reduced density ρ_r. The corresponding number density in the volume of 1 nm^3 is represented in the top axis.

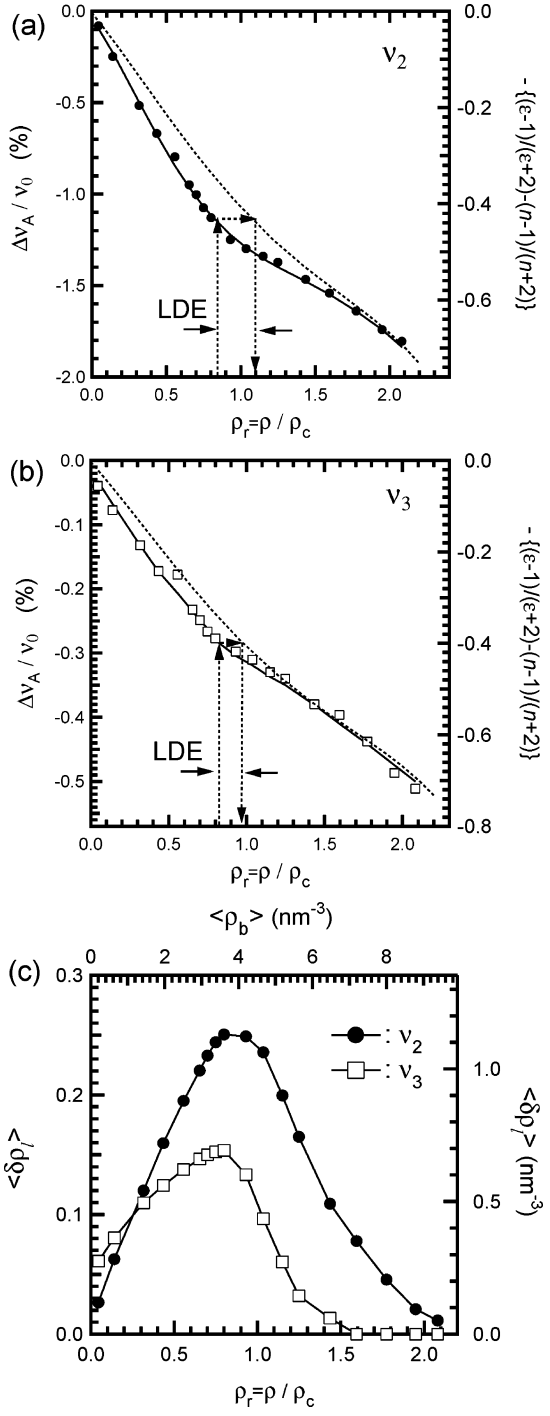

Figure 11. Attractive shift of (a) ν_2 and (b) ν_3 modes at the reduced temperature $T_r = 1.02$ as a function of reduced density ρ_r, analyzed by the Onsager reaction filed. (c) Local density enhancement (LDE) in the neat condition. Units of the local density enhancement and bulk density are reduced density ρ_r. The corresponding number density in the volume of 1 nm^3 is represented in the top axis.

supercritical CHF_3.[34] As a result, the value of Figure 11 is in agreement with that theoretical result, considering the electric interaction among polar CHF_3 molecules. Considering the nature of CHF_3 and the coincidence between the value of Figure 11 and the reported theoretical study, it is suggested that the value of Figure 11 seems to be suitable for polar molecules such as CHF_3. Thus, in the following discussion the local density enhancement obtained from the latter analysis is used in the present study.

Briefly, let us introduce the other studies relating to the local density enhancement of *neat supercritical fluids*. The large critical anomalies of Raman spectral width and frequency for supercritical O_2 were interpreted as the enhancement of local density.[37] Similar anomalies recently have been observed in the vibrational Raman spectra of supercritical N_2 at very close to the critical point,[66] although such an anomaly was not observed in a previous study relatively far from the critical temperature.[67] Nonlinear density dependences were also observed for the widths and shifts of Raman spectra of supercritical CO_2 at T_r

= 1.02−1.06. Nonlinearities were found to become most significant where the density inhomogeneity is greatest.[43] A study of a two-dimensional LJ fluid by MD simulation evaluated the local density enhancement as a function of bulk density.[31] A study of MC simulation of a three-dimensional LJ fluid showed subtle or no enhancement from the results of a linear local-coordination number.[32] The linear density dependences for spectral shifts of the C−H and C−C stretching modes of ethane were interpreted as a lack of local density enhancement at T_r = 1.02.[38,39] In a recent theoretical study, local density enhancement was clearly computed by the use of an inhomogeneous integral equation theory.[33] That paper found that the magnitudes of enhancement sensitively change with the kinds of intermolecular potentials, and the well depths of potential and temperature are concluded to play important roles in the value of local density enhancement of neat systems. Also, the latest theoretical study clearly found that the value of local density augmentation of a polar fluid, CHF_3, becomes larger than that of a nonpolar one, C_2H_6.[34] In that paper, dipole−dipole interaction is thought to increase the value of local density. On the basis of these recent theoretical and the present experimental results, it is natural to interpret that the local density enhancement exists in neat supercritical fluids of polar and nonpolar molecules, and that the amounts of local density enhancement depend on the degree of intermolecular interactions.

As another feature, the local density enhancement becomes maximum around $\rho_r = 0.8$ at $T_r = 1.02$. At the same density and temperature of supercritical CHF_3, specific features are commonly observed: the maximum local density enhancement investigated by simulation,[34] the maximum spectral width in Figure 7, the nonlinear shift as a function of the reaction field in Figure 8, the nonlinear shifts of electronic spectra as a function of the reaction field,[15] and the minimum rotational relaxation time.[68,69] Briefly, let us discuss these specificities by comparing them with the long-range structure of neat supercritical CHF_3. According to SAXS measurements,[10] the Ornstein−Zernike correlation length of supercritical CHF_3 was obtained as 1.6 nm at $\rho_r = 0.8$ and $T_r = 1.02$. The molecular size of CHF_3 is estimated to be 0.43 nm by van der Waals volume,[63] and the first and second solvent shells reach about 1.3 and 2.1 nm, respectively. Under these situations, the correlation length becomes longer than the first solvent shell and shorter than the second. That is, as the correlation length grows to such a scale, the local structure of such a spatial size significantly affects the vibrational, rotational,[68,69] and electronic[15] transitions in supercritical CHF_3.

V.C. Sensitivity of Vibrational Mode to Dielectric Surrounding the Vicinity of a Vibrating Molecule. As shown in Figure 11, the value of local density enhancement obtained from the ν_2 mode becomes larger than that from the ν_3. In the present study, the value of enhancement is obtained from the shift amounts of vibrational spectra, depending on density. The vibrational transition energy, as well as rotational and electronic energies, are affected differently by the dielectric surrounding at the same density and temperature conditions. For example, it was found that the spectral shifts of $\pi-\pi^*$ and n-π^* transitions of benzophenone show different density dependences in the supercritical fluid even though they have the same density and temperature.[70] The shift amount of the vibrational spectrum is also expected to show a different density dependence for each vibrational mode at the same thermodynamic condition.

We consider the attractive spectral shift in order to discuss the mode dependence of local density enhancement. Tables 3 and 4 summarize various systems for the attractive shifts of different vibrational modes in high-pressure conditions. The tables show that there are modes giving large or small attractive shifts regardless of whether the molecule, temperature, and pressure are the same. This mode dependence reflects a sensitivity of attractive interaction of vibrational mode against the dielectric surrounding in the vicinity of a vibrating molecule. In this situation, the present stretching mode is much affected by the dielectric surrounding and becomes more sensitive to the fluid than the deforming mode.

TABLE 4: Attractive Shift Parameters of Several Nonpolar and Polar Molecules

molecule	mode	C_a (cm^{-1} nm^3)
nonpolar		
N_2[a]	N−N stretch	−0.13
CH_4[a]	C−H stretch	−0.59
C_2H_6[a]	C−C stretch	−0.28
	C−H stretch	−0.96
isobutylene[b]	C=C stretch	−1.4
	C−C stretch	−0.50
cyclohexane[c]	C−H stretch	−0.59
polar		
acetone[b]	C=O stretch	−3.0
CH_3OH[d]	C−H stretch	−1.7
CH_3CN[e]	C−H stretch	−1.6
	C−N stretch	−1.5
	C−C stretch	−0.3
CH_3CN (in CCl_4)[e]	C−H stretch	−3.1
	C−N stretch	−2.3
	C−C stretch	
furan[f]	ring	−1.2

[a] Reference 38. [b] The C_a value is obtained with data from ref 51. [c] Reference 58. [d] The C_a value is obtained with data from ref 53. [e] The C_a value is obtained with data from ref 59. [f] The C_a value is obtained with data from ref 55.

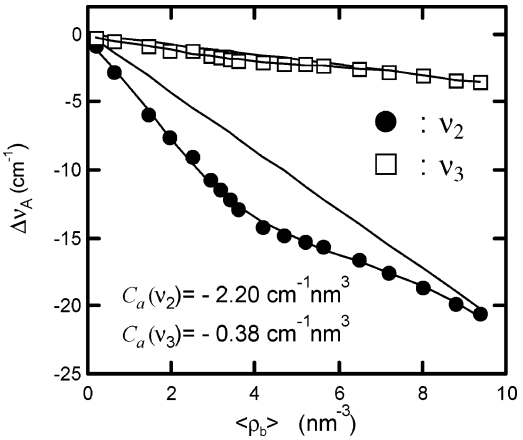

Figure 12. Attractive shift parameter C_a obtained from the slope of the linear line.

To understand the sensitivity of the vibrational mode, we discuss the attractive shift parameter C_a. On the basis of the SC model described in eq 17, the C_a was obtained from the slope as shown in Figure 12. The values of ν_2 and ν_3 modes are estimated to be −2.2 and −0.38 cm^{-1} nm^3, respectively. Table 4 lists the attractive shift parameters of several vibrational modes. Note that polar molecules such as acetone or CH_3CN show similar C_a values to the ν_2 mode of CHF_3 in the present study, whereas the value of the ν_3 mode is similar to those of nonpolar molecules.

The attractive shift parameter is expressed by dispersion and dipole−dipole terms as follows[59]

$$C_a = -(A_\alpha \alpha + A_\mu \mu^2) \propto -\left(\left(\frac{\partial \alpha}{\partial Q}\right)\alpha + \left(\frac{\partial \mu}{\partial Q}\right)\mu^2\right) \quad (19)$$

TABLE 5: Shift Amounts of Experimental Net, Calculated Repulsive, and Empirical Attractive Shifts as a Function of Pressure, Density, and Packing Fraction at Reduced Temperatures $T_r = T/T_c = 1.04$ and 1.06

				ν_2			ν_3		
pressure (MPa)	ρ (g cm^{-3})	$\rho_r = \rho/\rho_c$	packing fraction (%)	$\Delta\nu/\nu_0$ (%)	$\Delta\nu_R/\nu_0$ (%)	$\Delta\nu_A/\nu_0$ (%)	$\Delta\nu/\nu_0$ (%)	$\Delta\nu_R/\nu_0$ (%)	$\Delta\nu_A/\nu_0$ (%)
				$T_r = 1.04$					
0.80	0.02	0.04	0.8	−0.04	0.018	−0.06	−0.010	0.020	−0.030
2.20	0.07	0.13	2.5	−0.19	0.019	−0.21	−0.039	0.022	−0.061
3.52	0.13	0.25	4.6	−0.38	0.022	−0.40	−0.083	0.025	−0.108
4.54	0.20	0.38	7.1	−0.55	0.025	−0.58	−0.119	0.028	−0.147
5.05	0.25	0.48	8.8	−0.67	0.028	−0.69	−0.147	0.031	−0.179
5.34	0.29	0.55	10.2	−0.76	0.030	−0.79	−0.166	0.034	−0.199
5.63	0.34	0.64	11.9	−0.87	0.034	−0.91	−0.196	0.037	−0.233
5.92	0.40	0.77	14.2	−1.01	0.038	−1.05	−0.225	0.042	−0.266
6.21	0.49	0.93	17.2	−1.14	0.046	−1.18	−0.243	0.049	−0.293
6.47	0.57	1.08	20.0	−1.22	0.054	−1.27	−0.263	0.058	−0.321
6.76	0.64	1.21	22.4	−1.28	0.063	−1.34	−0.280	0.066	−0.347
7.15	0.70	1.33	24.6	−1.32	0.071	−1.39	−0.285	0.075	−0.360
7.65	0.75	1.42	26.4	−1.37	0.080	−1.45	−0.299	0.083	−0.382
9.55	0.85	1.62	29.9	−1.45	0.099	−1.55	−0.316	0.101	−0.417
13.89	0.95	1.81	33.5	−1.53	0.124	−1.66	−0.338	0.125	−0.462
20.00	1.03	1.96	36.2	−1.60	0.147	−1.74	−0.352	0.146	−0.498
25.00	1.07	2.04	37.8	−1.63	0.162	−1.79	−0.361	0.159	−0.520
				$T_r = 1.06$					
0.81	0.02	0.04	0.8	−0.04	0.018	−0.05	−0.013	0.020	−0.033
3.08	0.10	0.20	3.7	−0.31	0.021	−0.33	−0.086	0.024	−0.110
4.91	0.21	0.40	7.4	−0.59	0.026	−0.62	−0.157	0.029	−0.187
5.83	0.30	0.58	10.7	−0.81	0.032	−0.85	−0.210	0.035	−0.246
6.20	0.36	0.68	12.6	−0.93	0.036	−0.97	−0.236	0.039	−0.275
6.58	0.43	0.81	15.0	−1.06	0.041	−1.10	−0.265	0.045	−0.309
6.77	0.46	0.88	16.3	−1.11	0.044	−1.15	−0.282	0.048	−0.330
6.99	0.51	0.97	17.9	−1.17	0.049	−1.21	−0.290	0.052	−0.343
7.21	0.55	1.05	19.4	−1.21	0.053	−1.26	−0.292	0.057	−0.349
8.36	0.70	1.34	24.8	−1.35	0.074	−1.42	−0.323	0.077	−0.400
10.00	0.80	1.53	28.3	−1.43	0.091	−1.52	−0.349	0.094	−0.443
13.15	0.90	1.71	31.6	−1.50	0.112	−1.62	−0.358	0.114	−0.471
20.00	1.00	1.90	35.2	−1.59	0.141	−1.73	−0.375	0.140	−0.515
24.00	1.04	1.98	36.6	−1.62	0.153	−1.77	−0.379	0.152	−0.531

where α is the polarizability and μ dipole is the moment of a molecule. Since polarizability and dipole moment are common in a molecule, the difference in the value of C_a for each vibrational mode is considered to be the values of polarizability and dipole moment differentiated along vibrational coordinates. The value of $\partial\alpha/\partial Q$ of an isolated CHF_3 molecule was obtained from normal coordinate analysis by Gaussian 98, and the values of $\partial\mu/\partial Q$ were reported as follows: $(\partial\alpha/\partial Q)_{\nu 2}/(\partial\alpha/\partial Q)_{\nu 3} = 1.5$ and $(\partial\mu/\partial Q)_{\nu 2}/(\partial\mu/\partial Q)_{\nu 3} = 1/(-1.2)$.[71] All these values contribute toward a smaller C_a in the ν_3 mode than in the ν_2. This tendency is in accordance with the experimental results. That is, the curvature of the vibrational potential is opened by the increase in density, and this increased ν_2 mode exceeds the ν_3 mode. The ν_2 mode is much exerted by attractive intermolecular interactions. Under these conditions, it was considered that the sensitive mode offers a relatively higher degree of local density enhancement.

V.D. Temperature Dependence of Local Density Enhancement. We then measured the Raman spectra of ν_2 and ν_3 modes at different temperatures in the supercritical region. As shown in Figure 7, insignificant temperature dependence is observed in the spectral shifts. As listed in Table 5, the spectral shifts are also analyzed by decomposing them into attractive and repulsive components at $T_r = 1.04$ and 1.06. As described in eq 8, the repulsive shift becomes larger as the temperature increases. These temperature-led increases become small, and those at $T_r = 1.04$ and 1.06 are less than 2% and 4%, respectively, in contrast to the value at $T_r = 1.02$ at the same density. Both the net shift from the experiment and the repulsive shift from the calculation show insignificant temperature dependences in the present experimental range. As a result, we can say that the attractive shift's dependence on temperature is insignificant.

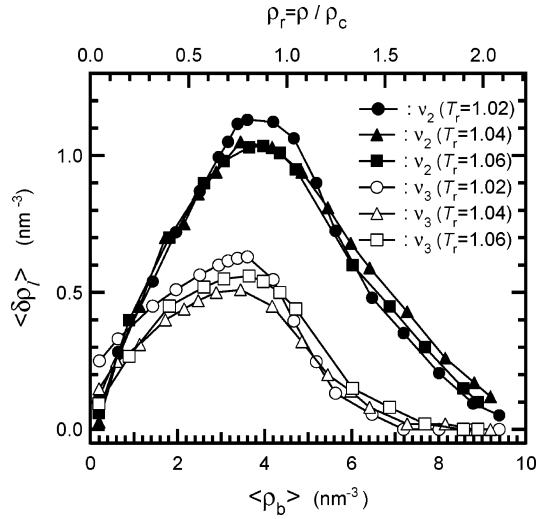

Figure 13. Local density enhancement for ν_2 and ν_3 modes obtained from the reaction filed analysis at the supercritical region at $T_r = 1.02$, 1.04, and 1.06.

We also estimated the local density enhancements at $T_r = 1.04$ and 1.06 using the data of attractive shifts and reaction fields at those temperatures. The results of the local density enhancements are displayed in Figure 13. The obtained values do not depend much on the temperature because of the insignificant temperature dependence of the attractive shift. On the contrary, the long-range inhomogeneity observed by SAXS

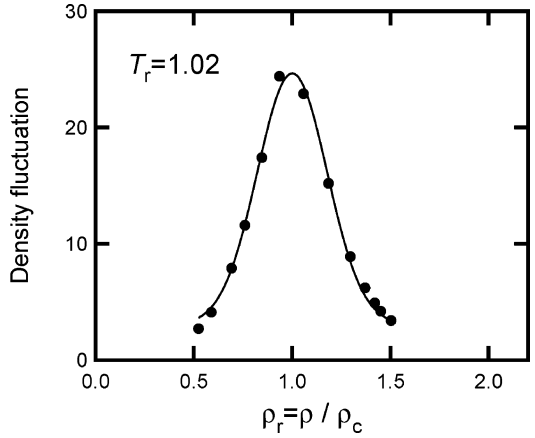

Figure 14. Density fluctuation of supercritical CHF_3 at the reduced temperature $T_r = T/T_c = 1.02$. The values are obtained from measurements of small-angle X-ray scattering and thermodynamic calculations of supercritical CHF_3 in ref 10.

measurement shows significant temperature dependence; the obtained correlation lengths of supercritical CHF_3 at $\rho_r = 1.0$ of $T_r = 1.02$, 1.04, and 1.06 are 2.0, 1.5, and 1.2 nm, respectively.[10] Briefly, let us discuss the difference in temperature dependence between short-range and long-range inhomogeneity. For each experimental condition, the SAXS detects long-range inhomogeneity that is larger than an order of nanometer, whereas the data from vibrational Raman spectroscopy reflect a short-range structure in the neighborhood of a vibrating molecule. In contrast to the molecular size of 0.43 nm, the sizes of inhomogeneities probed by SAXS and Raman become large and small, respectively. Under this condition, it is considered that the structure around a vibrating molecule does not change much in the present temperature range, although the structure of a large scale surrounding molecule sensitively changes. In a similar case of insignificant temperature dependences, the spectral shift and width of vibrational Raman spectra of neat supercritical CO_2 does not depend much on temperatures in the range of $1.02 \leq T_r \leq 1.06$.[43] In this case, it is also observed that the long-range inhomogeneity of supercritical CO_2 is sensitively changed by temperatures in the range of $1.02 \leq T_r \leq 1.06$.[10] Accordingly, it is revealed that a significant difference of temperature dependences exits in the short-range and long-range inhomogeneity of neat supercritical fluids.

V.E. Correlation between Short-Range and Long-Range Inhomogeneities. In condensed phases, the data of vibrational Raman spectra are reflected by continuous intermolecular interactions in the vicinity of a vibrating molecule; measured spectra show an ensemble average of each molecule under interactions at the first or second nearest neighbors.[64,65] As mentioned in Section V.B, the sizes of first and second solvent shells of CHF_3 molecules become about 1.3 and 2.1 nm, respectively. In the present study, the local density enhancement represents a volume of 1 nm^3. When molecules are affected by solvent shells of such sizes, the volume of 1 nm^3 seems to be appropriate to characterize the surroundings of a vibrating molecule.

Let us discuss the relationship between short-range and long-range inhomogeneities of supercritical CHF_3 in the same thermodynamic states. For a long-range inhomogeneity, Figure 14 shows the density fluctuation of supercritical CHF_3, whose value is obtained from SAXS measurements and isothermal compressibility.[10] The density fluctuation is characterized by inhomogeneity in the mesoscopie and/or macroscopic scale, e.g. $l >$ an order of a few tens of nanometers. By comparing the profile of local density enhancement with the profile of density fluctuation, it is shown that there are several differences in features between short- and long-range inhomogeneities. First, the maximum density fluctuation is located near $\rho_r = 1.0$, whereas the local density enhancement becomes maximum around $\rho_r = 0.8$. As a result, the maximum short-range inhomogeneity is located at a lower bulk density than the long-range one. Second, the distribution of density fluctuation is almost symmetric in shape. The local density enhancement shows antisymmetric distribution, and the amount of the enhancement in the lower bulk density exceeds that of the higher one. Third, the distribution of local density enhancement becomes broader than that of density fluctuation. These three features that distinguish between the short- and long-range inhomogeneities are very similar to the results of MD simulation as a function of spatial size.[31] That is, (i) the position of the maximum local density enhancement shifts toward a lower density as the local region becomes smaller, (ii) the distribution of local density enhancement becomes antisymmetric as a probed region becomes smaller, and (iii) the local density enhancement shows a broad distribution. In this simulation, the local density enhancement was investigated by changing the spatial scale from 1.78σ to 4.72σ, where σ is the particle size consisting of L-J fluid. In the case of a CHF_3 molecule, the values of 1.78σ and 4.72σ reach about 0.8 and 2 nm by use of the van der Waals diameter, respectively. These sizes seem to resemble the values of the effective scale around a vibrating molecule, such as the sizes of the first and second solvent shells and the local volume used to obtain local density enhancement in the present study. Recently, similar size dependence of local density enhancement was examined by another simulation study, and the three features mentioned above for spatial size were also observed by evaluating the local density enhancement for the first and second solvent shells.[34]

As the description of long-range inhomogeneity, the density fluctuation is formulated by the number-density inhomogeneity as follow,[3,10−12]

$$\frac{\langle(\Delta N)^2\rangle}{\langle N\rangle} = \frac{\langle(N - \langle N\rangle)^2\rangle}{N} = \frac{I(0)}{Z^2\langle N\rangle}\left(\frac{N}{V}\right)\kappa_T k_B T \qquad (20)$$

where N is the number of molecules in volume V, $\langle N\rangle$ is its ensemble-averaged value, $I(0)$ is the scattering intensity at wave vector $k = 0$, Z is the number of electrons of a molecule, and κ_T is the isothermal compressibility. According to eq 20, the value of density fluctuation is obtained from a measurement of scattered intensity at $k = 0$ or from the value of κ_T by the use of the state equation with $P-V-\rho-T$ relations. The obtained values of density fluctuations are thus expressed by an ensemble-averaged inhomogeneity in the mesoscopic or macroscopic scale, e.g., $l >$ an order of a few tens of nanometers. These values characterize well the long-range inhomogeneity. The local density enhancement, however, characterizes the density inhomogeneity in the short range, i.e., on the order of a volume of 1 nm^3. When the local structure in the vicinity of a vibrating molecule is discussed, the short-range inhomogeneity is more suitable, because the vibrational Raman spectrum is given by an ensemble average of each vibrating molecule under continuous intermolecular interactions around the first or second nearest neighbors. This discussion is fruitful for determining a way to describe the local volume of a vibrating molecule, which is required to calculate inhomogeneous width (next section).

V.F. Comparison of Experimental Spectral Width with Calculated Homogeneous and Inhomogeneous Widths. As

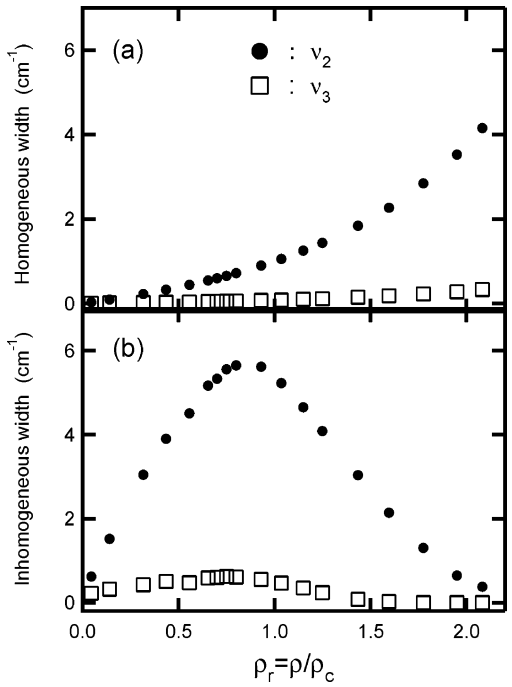

Figure 15. (a) Calculated homogeneous width of ν_2 and ν_3 modes in the supercritical state at the reduced temperature $T_r = 1.02$ as a function of reduced density. (b) Empirically calculated inhomogeneous widths at $T_r = 1.02$ as a function of the density.

mentioned in Section IV.B, the spectral broadening in the condensed phases arises from both dynamic and static effects, which are expressed respectively by homogeneous and inhomogeneous broadening. Although the deconvolution between the homogeneous and inhomogeneous widths has been recently performed by multidimensional nonlinear spectroscopy in time domain, deconvolution of those widths by experiment with linear spectroscopy seems to be difficult.[72] Thus, we calculated theoretically the homogeneous and inhomogeneous widths of supercritical CHF_3 as a function of density by using the SC model. The calculated widths in both vibrational modes are compared with the widths obtained from experiments.

The homogeneous width is generally described as follows

$$\Gamma = \frac{1}{\pi T_2} = \frac{1}{\pi T_2^*} + \frac{1}{2\pi T_1} + \Gamma_{or} \qquad (21)$$

where Γ is the width of the Lorentzian shape of a vibrational spectrum, T_2 is the homogeneous dephasing time, T_2^* is the pure dephasing time, T_1 is the population relaxation time, and Γ_{or} is the width by orientation relaxation.[72−74] In the present measurement, the value of Γ_{or} is neglected, because the spectra of ν_2 and ν_3 modes consist of the isotropic components as shown in Figure 3. We focus on the dephasing component, because the vibrational dephasing process, which is faster than the vibrational population relaxation, has been generally considered a principal contribution to the spectral width in condensed phases. As a result, the homogeneous width here is treated as the width given by vibrational dephasing.

As shown in Figure 15a, the calculated homogeneous width is obtained at $T_r = 1.02$ as a function of density. The homogeneous widths of both vibrational modes are monotonically broadened. An increase in collision frequency by the increase in density accelerates the dephasing process, resulting in the broadening of the homogeneous width. As another feature, the homogeneous width of the ν_2 mode is larger than that of the ν_3 mode. Equations 11−14 confirm that this difference is attributable mainly to the value of Δq, which is related to the vibrational anharmonicity. Large anharmonicity has been considered to contribute largely to vibrational dephasing. In the present study, as listed in Table 1, the value of the anharmonic force constant of the ν_2 mode is much larger than that of the ν_3 mode. Thus, it is interpreted that the homogeneous width of the ν_2 mode becomes broader than that of the ν_3 mode.

Next, we discuss the inhomogeneous widths of both vibrational modes as functions of density. These widths are empirically calculated in the following manner. According to eqs 15 and 16, three parameters are required to obtain an inhomogeneous width: the amount of attractive shift ($\Delta\nu_A$), the average number of molecules (N) in the local volume, and the difference (ΔN) between the average and the effective numbers of molecules in the volume. The first parameter is obtained in Section V.A. The second and third are utilized as the average number of molecules in the volume of 1 nm^3 and the local density enhancement in 1 nm^3, respectively, as described in the previous section. Thus the calculated inhomogeneous width is shown in Figure 15b as the data at $T_r = 1.02$. The following features are obtained. First, the inhomogeneous width of the ν_2 band is larger than that of the ν_3 band. Second, the anomaly of inhomogeneous width appears around $\rho_r = 0.8$.

We compare the values of experimental results with those of calculated ones. As shown in Figure 15, the inhomogeneous width is larger than the homogeneous width in almost density range of the current study. As a result, it is considered that the spectral broadening observed from the experiments consists mainly of the inhomogeneous component. This means that the major contribution to the spectral broadening is due to attractive interactions because of the inhomogeneous width brought by attractive interactions in the SC model. As for spectral shift, a similar feature is observed. Figure 9 shows that the attractive component is the major contribution to the amount of a shift. On the basis of the present experimental and theoretical results, accordingly, it can be concluded that the attractive interactions contribute dominantly to both of the vibrational frequencies and the spectral widths for ν_2 and ν_3 modes of supercritical CHF_3 at all densities and temperatures in the present ranges.

As for the other features of experimental values of widths, specific density dependences are found, including the anomaly around $\rho_r = 0.8$ and the plateau at higher densities. To understand these features, we carry out the convolution of calculated homogeneous and inhomogeneous widths. The result is shown in Figure 16. It should be noted that the convoluted profiles agree with the experimental values. Both the values and profiles in the calculations are in accordance with the experimental results. Consequently, the anomaly in the experimental results is attributed mainly to density inhomogeneity. It is interpreted that the plateau is generated by both the increase in homogeneous width and the decrease in inhomogeneous width. This means that the fast modulation becomes manifest by the increase in density, and the slow modulation gradually becomes insignificant. Another feature seen is that the width of the ν_2 mode broadens at $\rho_r = 0$. This is obviously expected as an incidence of intramolecular vibrational relaxation at the limit of density = 0, for example, intramolecular vibrational energy transfer to the other vibrational modes or rotational populations. As shown in Figure 16, the widths of 15 and 0.7 cm^{-1}, which are assumed to be intramolecular relaxations at $\rho_r = 0$, are tentatively added into the calculated widths of the ν_2 and ν_3 modes, respectively.

The temperature dependence of width is also compared with the calculated one in the range of $T_r = 1.02$ to 1.06. In this

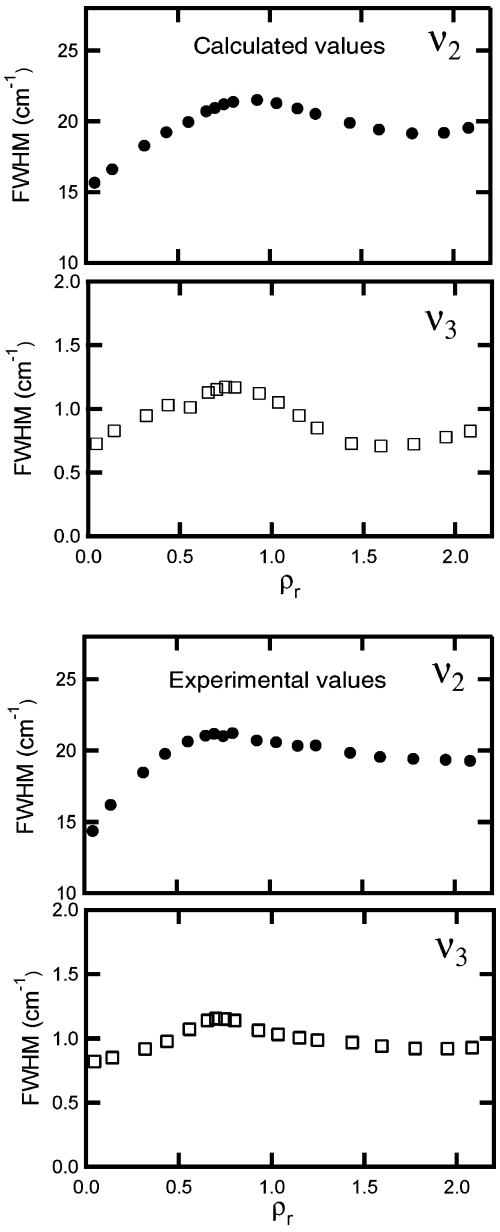

Figure 16. Total calculated widths of ν_2 and ν_3 modes obtained from the convolution of homogeneous and inhomogeneous widths. The spectral widths at the reduced density $\rho_r = 0$, the values of 15 and 0.7 cm^{-1}, which are assumed to be intramolecular vibrational relaxations at $\rho_r = 0$, are tentatively added into the calculated widths of the ν_2 and ν_3 modes, respectively.

range, the broadening of the homogeneous widths of ν_2 and ν_3 modes is calculated to be about 3% and 6%, respectively. Thus, the temperature dependence of the homogeneous case is insignificant. For the case of inhomogeneous width the dependence also becomes small, because the parameters required to obtain the inhomogeneous width by eqs 15 and 16, i.e., attractive shift and local density enhancement, are insensitive to the temperature change, as described in Sections V.A. and V.D. Accordingly, both homogeneous and inhomogeneous widths show insignificant temperature dependences. This tendency is in accordance with the experimental results.

VI. Concluding Remarks

We have investigated the short-range inhomogeneity of the polar polyatomic molecule by measuring the vibrational Raman spectra of the neat supercritical CHF_3 and analyzed the spectral shape and positions over a wide density range on the basis of the hard-sphere model. The spectral shifts were decomposed into attractive and repulsive components along vibrational coordinates, and the changes in attractive and repulsive energies were evaluated as functions of density. The measured spectral widths were compared with the calculated homogeneous and inhomogeneous widths. Accordingly, it was elucidated that the spectral shifts and widths of both vibrational modes are governed dominantly by the attractive intermolecular interactions at all densities in the range of temperature $1.02 \leq T/T_c \leq 1.06$ of the supercritical region. We have addressed the following conclusions of the local structure of neat supercritical CHF_3.

(i) The local structure in the vicinity of a vibrating CHF_3 molecule was characterized by the local density enhancement, which was evaluated by using the amounts of attractive vibrational shift and the Onsager reaction field. This estimation considered dielectric interactions of polar CHF_3 molecules. The estimated value was in agreement with the reported theoretical results,[34] considering the electronic interaction such as dipole−dipole interaction. The local density enhancement became maximum at around $\rho_r = 0.8$, where the various experimental and theoretical results commonly showed specific features. It was shown that the molecular motions are significantly affected at the density of $\rho_r = 0.8$, and the correlation length exceeds that of the first solvent shell.

(ii) The density dependences of spectral widths were analyzed by comparing the experimental values with the calculated widths. The experimental values agreed with the calculated widths in the present study, which were obtained from the convolution of the calculated homogeneous and inhomogeneous widths. The anomaly and plateau of width observed by experiments of density dependence were rationalized; thereby the former is given by density inhomogeneity due to attractive interaction, and the latter is given by both the increase in vibrational dephasing and the decrease in density inhomogeneity.

(iii) The temperature dependence of short-range inhomogeneity was investigated by analyzing the spectral widths and shift. The local structure in the vicinity of a vibrating molecule is insignificantly depended on the temperature. It was revealed that a significant difference of temperature dependences exits in the short-range and long-range inhomogeneity of neat supercritical fluids.

Acknowledgment. The authors thank Messrs. Miyagi and Shimokawa of the Machine Shop at Gakushuin University, for their discussions with us on the design of the optical cell, and Mrs. Otake and Mr. Hashizume, for their collaborations during measurement. K.S. thanks Prof. Maroncelli for the fruitful discussions, and also acknowledges a Collaboration Research grant for young researchers from the Graduate School of Science and Technology of Chiba University. This work has been partially supported by a grant-in-aid for Scientific Research from the Ministry of Education, Science, and Culture, Japan.

References and Notes

(1) Kajimoto, O. *Chem. Rev.* **1999**, *99*, 355.
(2) Tucker, S. C. *Chem. Rev.* **1999**, *99*, 391.
(3) Stanley, H. E. *Introduction to phase transitions and critical phenomena*; Oxford University Press: New York, 1971.
(4) Greer, S. C.; Moldover, M. R. *Annu. Rev. Phys. Chem.* **1981**, *32*, 233.
(5) Sengers, J. V.; Sengers, J. M. H. L. *Annu. Rev. Phys. Chem.* **1986**, *37*, 189.
(6) Maccabee, B. S.; White, J. A. *Phys. Rev. Lett.* **1971**, *27*, 495.
(7) Swinney, H. L.; Henry, D. L. *Phys. Rev. A* **1973**, *8*, 2587.
(8) Letaief, A.; Tufeu, R.; Garrabos, Y.; Neindre, B. Le. *J. Chem. Phys.* **1986**, *84*, 921.

(9) Lunacek, J. H.; Cannell, D. S. *Phys. Rev. Lett.* **1971**, *27*, 841.
(10) Nishikawa, K.; Morita, T. *Chem. Phys. Lett.* **2000**, *316*, 238.
(11) Nishikawa, K.; Kusano, K.; Arai, A. A.; Morita, T. *J. Chem. Phys.* **2003**, *118*, 1341.
(12) Nishikawa, K.; Ochiai, H.; Saitow, K.; Morita, T. *Chem. Phys.* **2003**, *286*, 421.
(13) Saitow, K.; Ochiai, H.; Kato, K.; Nishikawa, K. *J. Chem. Phys.* **2002**, *116*, 4985.
(14) Saitow, K.; Kajiya, D.; Nishikawa, K. *J. Am. Chem. Soc.* **2004**, *126*, 422.
(15) Kajimoto, O.; Fukutami, M.; Kobayashi, T.; Yamasaki, K. *J. Phys. Chem.* **1988**, *92*, 1347.
(16) Rice, J. K.; Niemeyer, E. D.; Dunbar, R. A.; Bright, F. V. *J. Am. Chem. Soc.* **1995**, *117*, 5832.
(17) Sun, Y.-P.; Benett, G.; Jonston, K. P.; Fox, M. A. *J. Phys. Chem.* **1992**, *96*, 10001.
(18) Mayer, D. J.; Motoyuki, S.; Fayer, M. D.; Cherayil, B. J. *J. Phys. Chem. B* **2000**, *104*, 2402.
(19) Schwarzer, D.; Troe, J.; Zerezke, M. *J. Chem. Phys.* **1997**, *107*, 8380.
(20) Benzeler, J.; Linkersdürfer, S.; Luther, K. *J. Chem. Phys.* **1997**, *106*, 4992.
(21) Heitz, M. P.; Maroncelli, M. *J. Phys. Chem. A* **1997**, *101*, 5852.
(22) Brenneccke, J. F.; Eckert, C. A. *AIChE J.* **1993**, *39*, 876.
(23) Randolph, W.; O'Brien, J. A. *Ind. Eng. Chem. Res.* **1996**, *35*, 19.
(24) Tucker, S. C.; Maddox, M. W. *J. Phys. Chem. B* **1998**, *102*, 2437.
(25) Song, W.; Biswas, R.; Maroncelli, M. *J. Phys. Chem. A* **2000**, *104*, 6924.
(26) Egorov, S. A. *J. Chem. Phys.* **2002**, *116*, 2004.
(27) Eckert, C. A.; Knutson, B. L.; Debenedetti, P. G. *Nature* **1996**, *386*, 313.
(28) Zang, J.; Roek, D. P.; Chateauneuf, J. E.; Brennecke, J. F. *J. Am. Chem. Soc.* **1997**, *119*, 9980.
(29) Wada, N.; Saito, M.; Kitada, D.; Smith, R. L., Jr.; Inomata, H.; Arai, K.; Saito, S. *J. Phys. Chem. B* **1997**, *101*, 10918.
(30) Knutson, B. L.; Tomasco, D. L.; Eckert, C. A.; Debenedetti, P. G.; Chialvo, A. A. *Supercritical Fluids Technology*; ACS Symp. Ser. No. 488; Bright, F. V., McNanlly, M. E., Eds.; American Chemical Society: Washington, DC, 1992; p 60.
(31) Maddox, M. W.; Goodyear, G.; Tucker, S. C. *J. Phys. Chem. B* **2000**, *104*, 6248.
(32) Egorov, S. A.; Yethiraj, A.; Skinner, J. L. *Chem. Phys. Lett.* **2000**, *317*, 558.
(33) Egorov, S. A. *Chem. Phys. Lett.* **2002**, *354*, 140.
(34) Song, W.; Maroncelli, M. *Chem. Phys. Lett.* **2003**, *378*, 410.
(35) Saitow, K.; Otake, K.; Nakayama, H.; Ishii, K.; Nishikawa, K. *Chem. Phys. Lett.* **2003**, *368*, 209.
(36) Saitow, K.; Ohtake, H.; Sarukura, N.; Nishikawa, K. *Chem. Phys. Lett.* **2001**, *341*, 86.
(37) Clouter, M. J.; Kiefte, H.; Deacon, C. G. *Phys. Rev. A* **1986**, *33*, 2749.
(38) Ben-Amotz, D.; LaPlant, F.; Shea, D.; Gardecki, J.; List, D. *Supercritical Fluids Technology*; ACS Symp. Ser.No. 488; Bright, F. V., McNanlly, M. E., Eds.; American Chemical Society: Washington, DC, 1992; p 144.
(39) Egorov, S. A.; Skinner, J. L. *J. Phys. Chem. A* **2000**, *104*, 483.
(40) Gilliam, O. R.; Edwards, H. D.; Gordy, W. *Phys. Rev.* **1954**, *75*, 1014.
(41) Herzberg, G. *Molecular spectra and molecular structure. II. Infrared and Raman spectra of polyatomic molecules*; Krieger Publishing Company: New York, 1950.
(42) Bernstein, H. J.; Herzberg, G. *J. Chem. Phys.* **1948**, *16*, 30.
(43) Nakayama, H.; Saitow, K.; Sakashita, M.; Ishii, K.; Nishikawa, K. *Chem. Phys. Lett.* **2000**, *320*, 3223.
(44) Rubio, R. G.; Zollweg, J. A.; Palance, J. M. G.; Calode, J. C. G.; Miller, J.; Streett, W. B. *J. Chem. Eng. Data* **1991**, *36*, 171.
(45) Ruoff, A.; Burger, H.; Biedermann, S. *Spectrochim. Acta A* **1971**, *27*, 1359.
(46) Onsager, L. J. *J. Am. Chem. Soc.* **1936**, *58*, 1486.
(47) McRae, E. G. *J. Phys. Chem.* **1957**, *61*, 526.
(48) Akimoto, S.; Kajimoto, O. *Chem. Phys. Lett.* **1993**, *209*, 268.
(49) Tozaki, K.; Kurino, S.; Kudoh, J.; Nishikawa, K. In preparation.
(50) Kajiya, D.; Saitow, K.; Nishikawa, K. In preparation.
(51) Schweizer, K. S.; Chandler, D. *J. Chem. Phys.* **1982**, *76*, 2296.
(52) Zakin, M. R.; Herschbach, D. R. *J. Chem. Phys.* **1986**, *95*, 2376.
(53) Zakin, M. R.; Herschbach, D. R. *J. Chem. Phys.* **1988**, 89, 2380.
(54) Ben-Amotz, D.; Herschbach, D. R. *J. Phys. Chem.* **1993**, *97*, 2295.
(55) Lee, Y. T.; Wallen, S. L.; Jonas, J. *J. Phys. Chem.* **1992**, *96*, 4282.
(56) Jonas, J.; Lee, Y. T. *J. Phys. Condens. Matter* **1991**, *3*, 305.
(57) Zerda, T. W.; Thomas, H. D.; Bradley, M.; Jonas, J. *J. Chem. Phys.* **1987**, 86, 3219.
(58) Pan, X.; McDonald, J. C.; MacPhail, R. A. *J. Chem. Phys.* **1999**, *110*, 1677.
(59) Ben-Amotz, D.; Lee, M.-R.; Cho, S. Y.; List, D. J. *J. Chem. Phys.* **1992**, *96*, 8781.
(60) Maynard, A. T.; Wyatt, R. E.; Iung, C. *J. Chem. Phys.* **1995**, *103*, 8372.
(61) Oxtoby, D. W. *J. Chem. Phys.* **1979**, *70*, 2605.
(62) Fischer, S. F.; Laubereau, A. *Chem. Phys. Lett.* **1975**, *35*, 6.
(63) Edward, J. T. *J. Chem. Edu.* **1970**, *47*, 261.
(64) Oxtoby, D. W. *Adv. Chem. Phys.* **1979**, *40*, 1.
(65) Oxtoby, D. W. *Annu. Rev. Phys. Chem.* **1981**, *32*, 77.
(66) Musso, M.; Matthai, F.; Keutel, D.; Oehme, K. *J. Chem. Phys.* **2002**, *116*, 8015.
(67) Clouter, M. J.; Kiefte, H.; Ali, N. *Phys. Rev. Lett*, **1978**, *40*, 1170.
(68) Okazaki, S.; Matsumoto, M.; Okada, I.; Maeda, K.; Kataoka, Y. *J. Chem. Phys.* **1994**, *103*, 8594.
(69) Song, W.; Patel, N.; Maroncelli, M. *J. Phys. Chem. B* **2002**, *106*, 8783.
(70) Bennett, G. B.; Johnston, K. P. *J. Phys. Chem.* **1994**, *98*, 441.
(71) Kondo, S.; Saeki, S. *J. Chem. Phys.* **1981**, *74*, 6603.
(72) Fayer, M. D., Ed. *Ultrafast Infrared and Raman spectroscopy*; Dekker: New York, 2001.
(73) Rector, K. D.; Fayer, M. D. *Int. Rev. Phys. Chem.* **1998**, *17*, 261.
(74) Fleming, G. R. *Chemical Application of Ultrafast Spectroscopy*; Oxford University Press: New York, 1986.